

3D velocity field reconstruction of gas-liquid two-phase flow based on space-time multi-scale binocular-PIV technology*

WANG Hongyi^{1**}, DOU Gongcheng², ZHANG Hao², ZHU Xinjun¹, and SONG Limei¹

1. Tianjin Key Laboratory of Intelligent Control of Electrical Equipment, School of Artificial Intelligence, Tiangong University, Tianjin 300387, China

2. Tianjin Key Laboratory of Intelligent Control of Electrical Equipment, School of Control Science and Engineering, Tiangong University, Tianjin 300387, China

(Received 18 January 2022; Revised 12 June 2022)

©Tianjin University of Technology 2022

For particle image velocimetry (PIV) technique, the two-dimensional (2D) PIV by one camera can only obtain 2D velocity field, while three-dimensional (3D) PIV based on tomography by three or four cameras is always complex and expensive. In this work, a binocular-PIV technology based on two cameras was proposed to reconstruct the 3D velocity field of gas-liquid two-phase flow, which is a combination of the binocular stereo vision and cross-correlation based on fast Fourier transform (CC-FFT). The depth of particle was calculated by binocular stereo vision on space scale, and the plane displacement of particles was acquired by CC-FFT on time scale. Experimental results have proved the effectiveness of the proposed method in 3D reconstruction of velocity field for gas-liquid two-phase flow.

Document code: A **Article ID:** 1673-1905(2022)10-0613-5

DOI <https://doi.org/10.1007/s11801-022-2007-8>

Particle image velocimetry (PIV) can accurately measure the instantaneous state of two-dimensional (2D) or three-dimensional (3D) flow field without contact, and provides an effective visual measurement method for fluid motion. The application field of PIV has gone beyond these traditional fluid motion fields^[1,2] and gradually extended to the fields of medicine, biology, oceanography and so on^[3-6]. Due to the high price of equipment and the demanding experimental environment, the application of PIV is greatly limited in the teaching^[7] and engineering^[8]. Therefore, it is imperative to study more convenient PIV technology.

Since ADRIAN^[9] first proposed the PIV technology, the research on multiphase flow has been deepening. SU et al^[10] combined PIV and deflected chromatography to reconstruct the 3D velocity and temperature field of eddy current combustion, and studied the characteristics of eddy current combustion. PEREZ et al^[11] proposed a method for 3D reconstruction of the velocity field in laminar flows using planar PIV data, and the obtained reconstructions of the streamwise velocity are reasonably accurate. HAMDI et al^[12] developed and realized the experiment device of impinging jet impinging slotted plate, and then used time resolved-tomographic particle image velocimetry (TR-TPIV) measurements technology

to analyze the 3D flow from the volumetric point of view. LI et al^[13] presented an experimental study of pore-scale flow dynamics of liquid CO₂ and water in 2D heterogeneous porous micromodels employing high-speed microscopic particle image velocimetry (micro-PIV), which facilitated pore-scale model development and validation.

But PIV measurement precision by tracer particles, measurement methods and various application scenario restrictions, how to improve the accuracy of flow field measurement, expanding its measuring range, and improving the image processing algorithm for the analysis of the complex flow field are still important research directions in the future PIV measurement technique^[14]. To solve the above problems, a binocular-PIV technique is innovated to reconstruct the 3D velocity flow field in this paper. By the proposed method, the plane displacement of particles is obtained by cross-correlation based on fast Fourier transform (CC-FFT) algorithm based on PIV images at adjacent time, and the particle depth is obtained by binocular vision based on PIV images from different visual angles at the same moment. Thus, the 3D velocity flow field could be reconstructed by binocular-PIV images on space-time multiscale.

The experimental system is shown in Fig.1. The hardware is used to capture particle images, which is mainly

* This work has been supported by the National Natural Science Foundation of China (Nos.51806150 and 61905178), the Program for the Research Project of Tianjin Municipal Education Committee (No.2019KJ020), and the Science and Technology Guiding Project of China Textile Industry Federation (No.2018086).

** E-mail: wanghongyi@tiangong.edu.cn

composed of tracer particles, lasers, flow field device, two charge coupled device (CCD) cameras, and computer. Bubbles rise up in the water in the transparent rectangular plexiglass pipe, and tracer particles are dispersed in the water. Double-pulse laser is selected as the light source of the system, which has the characteristics of high energy density and good divergence. Two cameras are set at a certain angle and calibrated by binocular calibration method, and then capture the particle images synchronously with a time interval Δt .

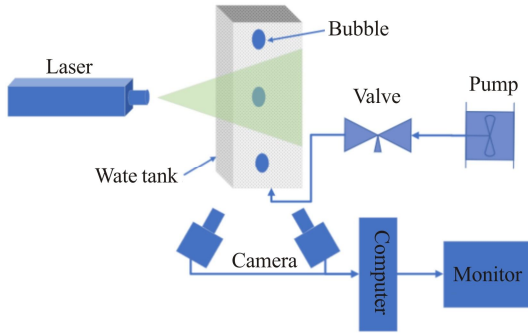


Fig.1 Binocular-PIV experimental system

The software system is used for particle image acquisition, image preprocessing, and 3D velocity flow field reconstruction. This paper focuses on the 3D velocity flow field reconstruction method with binocular PIV images. The 3D reconstruction process is shown in Fig.2.

In the calculation of particle depth, the key lies in the calculation of camera parameters and the acquisition of parallax matrix. We computed camera parameters by ZHANG's calibration method^[15], and obtained parallax map by binocular stereo vision method.

In the actual shooting environment, due to optical noise and camera gain, the light intensity received by the two cameras cannot be exactly the same, which results in a brightness difference between the left and right images. It brings great difficulty to stereo matching. Census stereo matching method based on the area stereo matching algorithm was applied for particle matching in this work^[16]. Census retains the position information of the pixels in the image, has good robustness to the brightness deviation, and can effectively reduce the mismatch caused by the brightness difference.

The main principle of the Census stereo matching method is encoding the image region and taking the two regions with the smallest coding distance as the matching pairs. As shown in Fig.3, a binary bit string could be obtained by comparing the matching point with the surrounding pixels using

$$\zeta[I(p), I(q)] = \begin{cases} 1, I(p) \leq I(q) \\ 0, I(p) > I(q) \end{cases} \quad (1)$$

where q is the gray value of the center point, and p is the gray value in the neighborhood.

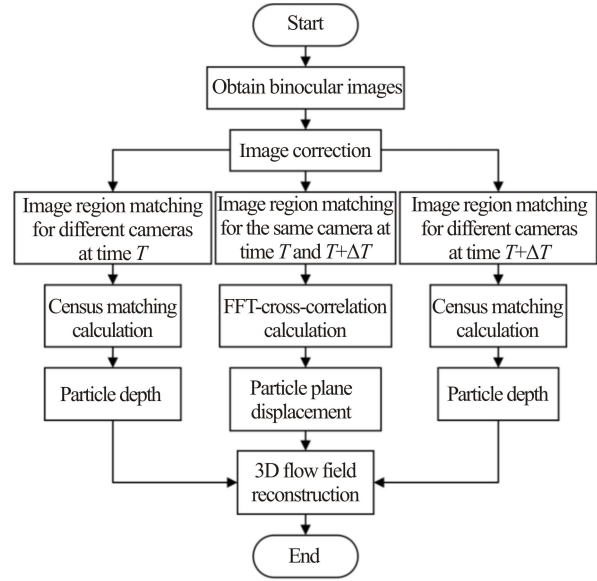


Fig.2 3D-PIV velocity field reconstruction flow chart

Then, the Hamming distance between two binary bit strings of different image regions from two PIV images could be calculated. The matching image region is of the minimum value of Hamming distance.

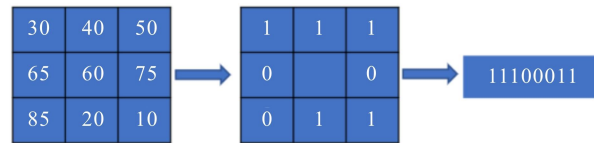


Fig.3 Census encoding process

Binocular stereo vision uses the parallax between the two cameras to simulate the human eyes for 3D reconstruction or depth measurement. After completing the stereo matching of the image, the parallax matrix of the two cameras could be calculated based on triangular ranging method.

Ideally, the mathematical model of binocular vision is shown in Fig.4. A point $P(x, y, z)$ in the 3D space represents an object in the world coordinate system. $P_1(x, y)$ and $P_2(x, y)$ represent the projection points of point P on the two cameras respectively. O_1 and O_2 are the optical centers of the two cameras, and the distance between which is the baseline distance B .

Assuming that the coordinates of each point in Fig.4 are in the camera coordinate system based on X -axis, ΔPP_1P_2 and ΔPO_1O_2 are similar, according to the principle of geometric similarity, the depth of point P can be calculated by

$$z = \frac{Bf}{d_1 + d_2}, \quad (2)$$

where f is the focal length of the camera, $O_1Q_1=d_1$, $O_2Q_2=d_2$, and d_1+d_2 is the parallax of the two cameras for point P . As can be seen, since B and f are definite, the

depth of the target point in the 3D space can be uniquely determined by the parallax.

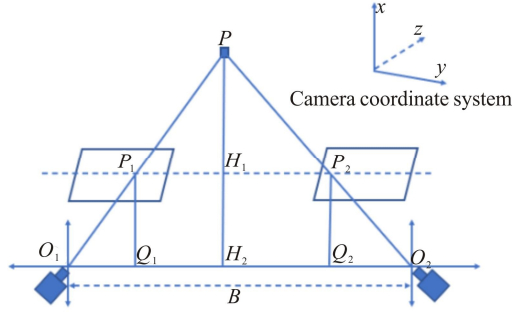


Fig.4 Image matching on special-scale based on the principle of triangular ranging

In the calculation of particle displacement, the algorithm of CC-FFT is applied to find the matching image region in this work. Compared with the census method used to match the spatial distribution characteristics of particles from different angles at the same time, the cross-correlation algorithm focuses on the change of particle density at adjacent time, so as to match the regional particles. As shown in Fig.5, the CC-FFT algorithm computes the cross-correlation matrix in the frequency domain, and then the cross-correlation matrix is inversely transformed into time domain.

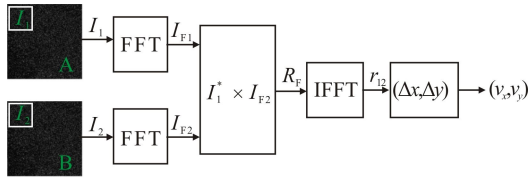


Fig.5 Processing course of CC-FFT algorithm

Using CC-FFT, the matching region in image B should be found for all template regions in image A. Assuming that the template region of particle image A is I_1 , while the area to be matched in image B is I_2 , the cross-correlation function $r_{12}(\tau_x, \tau_y)$ can be calculated by

$$r_{12}(\tau_x, \tau_y) = \iint I_1(x, y)I_2(x - \tau_x, y - \tau_y)dx dy. \quad (3)$$

If cross-correlation analysis of particle images is carried out directly, the 2D integral calculation requires a lot of time for computation, and cannot meet the requirements of real-time performance. In order to improve calculation efficiency, FFT is used to transform the image region into frequency domain.

The domain transformation by FFT can be expressed as

$$\begin{cases} I_{F1}(u, v) = \iint I_1(x, y)e^{-j(u x + v y)} dx dy \\ I_{F2}(u, v) = \iint I_2(x, y)e^{-j(u x + v y)} dx dy \\ R_F(u, v) = \iint r_{12}(\tau_x, \tau_y)e^{-j(u \tau_x + v \tau_y)} dx dy \end{cases} \quad (4)$$

According to the Wiener-Shinchin theorem, the

cross-correlation function in frequency domain can be expressed as

$$R_F(u, v) = I_{F1}^*(u, v) \times I_{F2}(u, v), \quad (5)$$

where * represents complex conjugation.

The cross-correlation matrix can be obtained by inverse FFT, as shown by

$$r_{12}(\tau_x, \tau_y) = \text{IFFT}\{I_{F1}^*(u, v) \times I_{F2}(u, v)\}. \quad (6)$$

As can be seen, the CC-FFT algorithm avoids complicated integration operation and could improve the computing speed of the cross-correlation matrix.

Once the cross-correlation matrix is acquired, the matching region can be determined by the maximum cross-correlation coefficient. For particle images, the relative displacement of particles in the region can be calculated, as shown in Fig.6.

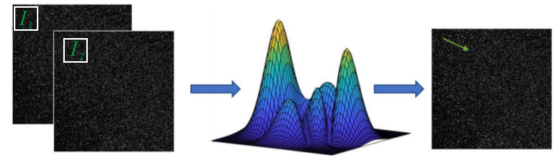


Fig.6 Image matching on time-scale based on CC-FFT

Using the above two methods, the region depth and the region displacement of particles image can be obtained respectively, as shown in Fig.7. The region depth Z_1 of the image at time T and the region depth Z_2 of the image at time $T + \Delta t$ are obtained on the space scale by the binocular stereo vision method. The region displacement X on time scale is calculated according to the CC-FFT algorithm.

Then the 3D velocity vector can be calculated based on the displacement and the depth by

$$MAPE_{3D} = \frac{100\%}{N} \left(\left| \frac{u_i - u'_i}{u_i} \right| + \left| \frac{v_i - v'_i}{v_i} \right| + \left| \frac{z_i - z'_i}{z_i} \right| \right), \quad (7)$$

where Δx , Δy and Δz denote the displacements of the tracer particle in the horizontal, vertical, and depth directions, respectively, while v_x , v_y , and v_z denote the instantaneous velocities of the tracer particle in the three directions, respectively. Finally, the 3D vector velocity field of the tracer particle could be obtained.

In order to verify the effectiveness of the method, this section simulates the multi-perspective particle distribution image of the 3D particle field. The particle fields of uniform flow and gradient flow are simulated in the 3D space and projecting them in different directions. The simulated fields are shown in Fig.8(a) and (c). The reconstructed results based on the projecting images by the proposed method are shown in Fig.8(b) and (d). The arrow vectors in different colors represent different velocities.

For different flow field data, root mean square error (RMSE) and mean absolute percentage error (MAPE)

were used to quantify the error detection results, which are shown in Tab.1. According to the 3D velocity field reconstruction results and average error, it can be seen that the velocity field reconstruction algorithm based on binocular PIV can better achieve the 3D flow field measurement.

The method proposed in this paper is further applied to the experimental measurement of gas-liquid two-phase flow, and the 3D liquid phase velocity field is reconstructed. During the experiment, the double-pulse laser illuminated the fluorescent particles in the flow field under the action of a trigger. Bubble was rising up in the water. At the the same time, the two cameras took pictures synchronously with a certain time interval. Binocular

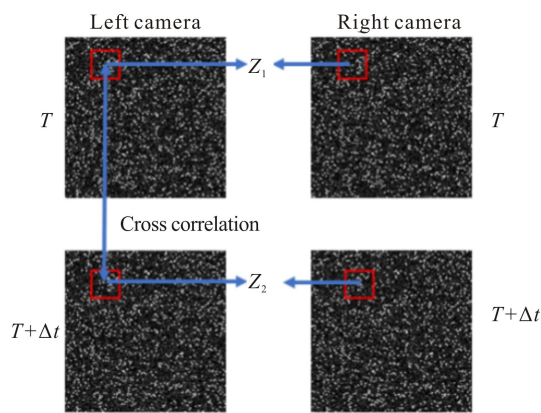
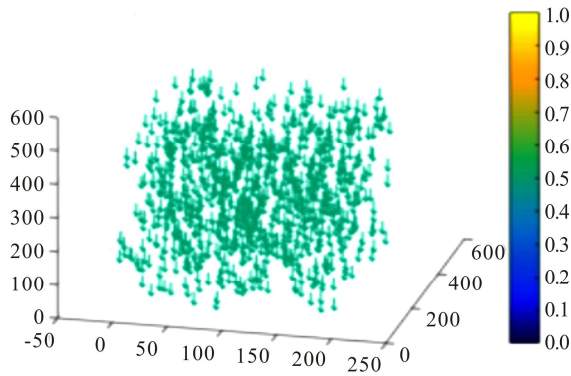
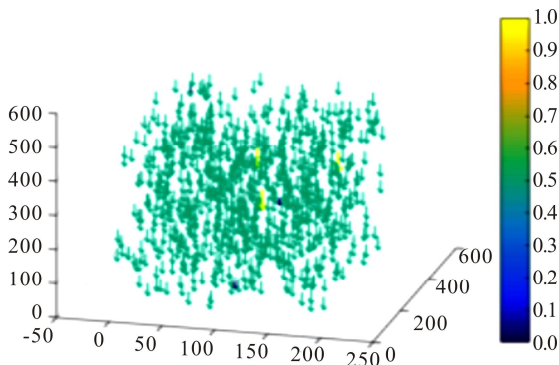


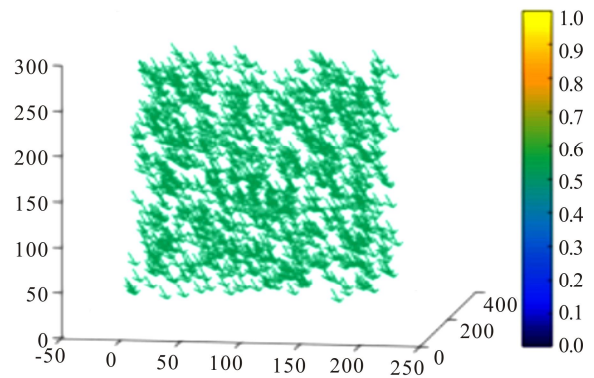
Fig.7 Binocular particle image region matching process



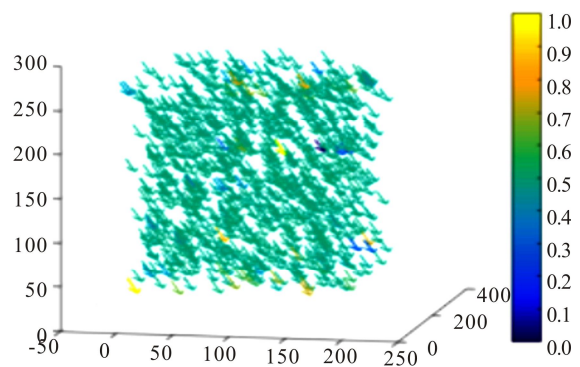
(a) Simulated fields



(b) Reconstructed fields



(c) Simulated fields



(d) Reconstructed fields

Fig.8 Experimental results of the simulated particle image

Tab.1 Reconstruction results of 3D velocity field of the simulated particle

	Uniform flow field	Gradient flow field	Average value
<i>RMSE</i>	0.66	0.81	0.735
<i>MAPE</i>	5.6%	11.4%	8.5%

particle images for bubble rising are shown in Fig.9(a). Velocity field for 2D plain based on left camera could be calculated by CC-FFT, which is shown in Fig.9(b). By combining the obtained particle depth information with the particle displacement vector, the 3D velocity field for the bubbly flow is reconstructed, as shown in Fig.9(c). The instantaneous velocity of the bubble flow field is displayed in different colors in the 3D field. In order to further improve the accuracy of 3D velocity field, some filtering methods were used to correct error vectors and outliers. The experiment result has shown that the reconstructed 3D flow field conforms its flow characteristics, has good continuity in the 3D space, and can well reflect the changes of the flow field.

In conclusion, the binocular-PIV system proposed in this paper realized the reconstruction of 3D velocity field for the bubbly flow. The 3D velocity vector was obtained by combining binocular stereo vision and CC-FFT algorithm

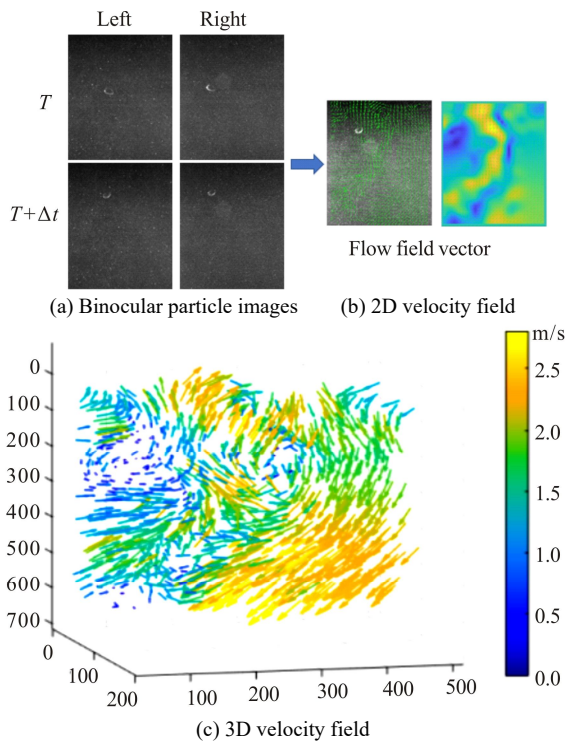


Fig.9 Binocular particle images and the reconstructed velocity field

on space-time multiscale. The proposed binocular-PIV system can use fewer cameras to solve the problem of 3D flow field reconstruction, which reduces the cost of PIV application and solves the problem of complex calculations. The proposed reconstruction method can also be extended to PIV image measurement at more angles to solve the problem of bubble occlusion and further improve the reconstruction accuracy.

Statements and Declarations

The authors declare that there are no conflicts of interest related to this article.

References

- [1] ADRIAN R J. Twenty years of particle image velocimetry[J]. *Experiments in fluids*, 2005, 39(2): 159-169.
- [2] YANG Z, WANG S, ZHENG J, et al. 20 kHz dual-plane stereo-PIV measurements on a swirling flame using a two-legged burst-mode laser[J]. *Optics letters*, 2020, 45(20): 5756.
- [3] DOROSHENKO A, LEE N, MACDONALD C, et al. Decline of influenza and respiratory viruses with COVID-19 public health measures: Alberta, Canada[J]. *Mayo clinic proceedings*, 2021, 96(12): 3042-3052.
- [4] TAN Z P, ALARCON R, ALLEN J, et al. Development of a high-speed plenoptic imaging system and application to marine biology PIV[J]. *Measurement science and technology*, 2020, 31(5): 054005.
- [5] SHU A P, RUBINATO M, QIN J P, et al. The hydrodynamic characteristics induced by multiple layouts of typical artificial M-type reefs with sea currents typical of Liaodong Bay, Bohai Sea[J]. *Journal of marine science and engineering*, 2021, 9(11): 1155.
- [6] LIU A H, LIN J J, ZHUANG Y J. PIV experimental study on the phase change behavior of phase change material with partial filling of metal foam inside a cavity during melting[J]. *International journal of heat and mass transfer*, 2022, 187: 122567.
- [7] MINICHELLO A, ARMIJO D, MUKHERJEE S, et al. Developing a mobile application-based particle image velocimetry tool for enhanced teaching and learning in fluid mechanics: a design-based research approach[J]. *Computer applications in engineering education*, 2021, 29(3): 517-537.
- [8] PAKHOV V V, STEPANOV R P, KUSYUMOV A N, et al. Investigation of aerodynamic performance of a multipurpose medium lift helicopter with different rear fuselage geometries[J]. *Russian aeronautics*, 2021, 64(2): 248-255.
- [9] ADRIAN R J. Scattering particle characteristics and their effect on pulsed laser measurements of fluid flow: speckle velocimetry vs. particle image velocimetry[J]. *Applied optics*, 1984, 23(11): 1690.
- [10] SU Y, ZHANG B, CHEN Y, et al. 3D velocity and temperature distribution measurement and characteristic analysis of swirling combustion[J]. *Measurement*, 2022, 193: 110949.
- [11] PEREZ J M, SASTRE F, CLAINCHE S L, et al. Three-dimensional flow field reconstruction in the wake of a confined square cylinder using planar PIV data[J]. *Experimental thermal and fluid science*, 2021: 110523.
- [12] HAMDJ J, ASSOUM H H, ALKHEIR M, et al. Analysis of the 3D flow of an impinging jet on a slotted plate using TR-Tomo PIV and proper orthogonal decomposition[J]. *Energy reports*, 2020, 6(S9): 158-163.
- [13] LI Y F, BLOIS G, KAZEMIFA R, et al. Quantifying the dynamics of water-CO₂ multiphase flow in microfluidic porous media using high-speed micro-PIV[C]//ASME 2020 International Mechanical Engineering Congress and Exposition, November 16-19, 2020, Virtual, Online. New York: ASME, 2020.
- [14] DU H, LI M G, LIU S X. Study of particle image velocimetry systems based on binocular vision[J]. *Systems engineering and electronics*, 2007, 29(11): 5.
- [15] ZHANG Z. A flexible new technique for camera calibration[J]. *IEEE transactions on pattern analysis and machine intelligence*, 2000, 22(11): 1330-1334.
- [16] ZABIH R, WOODFILL J. Non-parametric local transforms for computing visual correspondence[J]. *Lecture notes in computer science*, 1994, 801(1): 151-158.